Rheol Acta (2010) 49:1059–1069
DOI 10.1007/s00397-010-0480-7

ORIGINAL CONTRIBUTION

A smoothed particle hydrodynamics-based fluid model with a spatially dependent viscosity: application to flow of a suspension with a non-Newtonian fluid matrix

Nicos S. Martys · William L. George · Byong-Wa Chun · Didier Lootens

Received: 30 October 2009 / Revised: 16 August 2010 / Accepted: 18 August 2010 / Published online: 9 September 2010

Abstract A smoothed particle hydrodynamics approach is utilized to model a non-Newtonian fluid with a spatially varying viscosity. In the limit of constant viscosity, this approach recovers an earlier model for Newtonian fluids of Español and Revenga (Phys Rev E 67:026705, 2003). Results are compared with numerical solutions of the general Navier–Strokes equation using the "regularized" Bingham model of Papanastasiou (J Rheol 31:385–404, 1987) that has a shear-rate-dependent viscosity. As an application of this model, the effect of having a non-Newtonian fluid matrix, with a shear-rate-dependent viscosity in a moderately dense suspension, is examined. Simulation results are then compared with experiments on mono-size silica spheres in a shear-thinning fluid and for sand in a calcium carbonate paste. Excellent agreement is found between simulation and experiment. These results indicate that measurements of the shear viscosity of simple shear-rate-dependent non-Newtonian fluids may be used in simulation to predict the viscosity of concentrated suspensions having the same matrix fluid.

N. S. Martys (✉) · W. L. George
National Institute of Standards and Technology,
100 Bureau Drive, Stop 8615,
Gaithersburg, MD 20899-8615, USA
e-mail: nicos.martys@nist.gov

B.-W. Chun
Grace Construction Products,
Cambridge, MA 02140, USA

D. Lootens
SIKA Technology A.G.,
Tuffenwies 16, 8048 Zürich, Switzerland

Keywords Smoothed particle hydrodynamics · Suspension · Shear-thinning fluids · Non-Newtonian fluids

Introduction

The flow- and time-dependent properties of non-Newtonian fluids are important in many biological, environmental, and technological processes including blood flow, food processing, and the placement of concrete. In many cases, the non-Newtonian fluid of interest is a suspension of rigid bodies immersed in a matrix fluid. Such systems exhibit a wide variety of phenomena such as shear thinning (Larson 1999), shear thickening (Bender and Wagner 1996; Barnes 1989), shear banding (Moller et al. 2006; Fielding and Olmsted 2004), dilatancy (Barnes 1989), and jamming (Lootens et al. 2003). Most theoretical studies assume that the matrix fluid of the suspension is Newtonian, where the constitutive relation describes a linear stress evolution as a function of shear rate with zero yield stress. Except for the case of dilute (i.e., low-volume fraction) suspensions, the inherent complexity of suspensions makes it difficult to predict the rheological properties from purely theoretical means. Instead, there is an effort to develop computationally based models to help improve our understanding of complex fluids. The detailed modeling of suspension flow is challenging because the time evolution of a rigid body's motion entails keeping track of a moving boundary at the fluid-solid interface. Still, many advances have been made in understanding and predicting the flow properties of suspensions where the matrix fluid is Newtonian as an array of approaches

have been developed including traditional computational fluid dynamics, Stokesian dynamics (Foss and Brady 2000) and Lagrangian-based approaches like dissipative particle dynamics (DPD) (Hoogerbrugge and Koelman 1992; Boek et al. 1997; Martys 2005). However, for many suspensions of interest, the matrix fluid, for instance a cement paste (Flatt et al. 2004) or polymeric-based material, is non-Newtonian. Often such fluids can be described using Bingham, Herschel Bulkley, or power-law models that have a shear-rate-dependent stress or viscosity with a yield stress. The computational modeling of such suspensions is greatly complicated by the fact that local shear rates and hence the viscosity can widely vary throughout the suspension. This feature is not accounted for in current computational models of suspensions.

In this paper, a numerical model is presented for modeling non-Newtonian fluids with application to flow of a suspension with a non-Newtonian fluid matrix using a smoothed particle hydrodynamics (SPH)-based approach. This model builds on and, in some respects, is a synthesis of results found in Monaghan (2005) and Español and Revenga (2003). For this paper, the fluid modeled may be described as having a viscosity that is allowed to have a spatial dependence. That is, the viscosity may, for example, depend on the local shear rate or temperature which can, in turn, vary spatially. It is shown that the model agrees well with direct numerical solution of the general Navier–Strokes equation for an idealized Bingham model of Papanastasiou, in the cases of Couette and Poiseuille flow. As an application of this model, the effect of having a non-Newtonian fluid matrix, with a shear rate dependent viscosity in a moderately dense suspension, is then examined. Simulation results are compared with experimental data of monosized silica particles in a shear-thinning fluid matrix. We also consider the case of non-spherical particles where simulation results are compared with experiments on sand particles in a calcium carbonate paste. This paper is organized as follows. Firstly, the numerical equations for the simulation are derived and the computational model is then described. The simulation model is then validated for some simple flows like Couette and Poiseuille flow using the "regularized" Bingham model of Papanastasiou (1987) which has a shear-rate-dependent viscosity. Using the same model fluid, a sphere suspension is then simulated to understand the consequences of having a non-Newtonian fluid matrix. Next, comparison between experiment and simulations are given for the cases of monosize spherical silica particles in a shear-thinning fluid and finally for sand in a calcium carbonate/water paste.

Numerical model

The model presented in this paper is based on the SPH approach. SPH is a Lagrangian formulation of the Navier–Stokes equations that was originally developed by Gingold and Monaghan (1977) and Lucy (1977) to study astrophysical problems. Recent advances include the inclusion of thermal fluctuations (Español and Revenga 2003) in hydrodynamic flows and models describing viscoelastic fluids. While SPH has many guises, the approach used in this paper largely relies on the discretization of an integral representation of the Navier–Stokes equations. The basic idea is to construct an integral equation, composed of the fluid variables, and a specified weight function having properties such that when suitable dynamical variables are Taylor expanded in the integral, key parts of the Navier–Stokes equations are recovered. Once a satisfactory form of integrand is determined, the integral is represented as a discrete summation over a weighted set of points. Each point corresponds to a SPH "particle" which carries information related to local fluid properties (e.g., density, velocity...). For example, consider the Taylor expansion, about $\mathbf{r}$ of the following integral:

$$\begin{aligned}\int \mathrm{d}\mathbf{r}'\big(f(\mathbf{r}')-f(\mathbf{r})\big)\big(\mathbf{r}'-\mathbf{r}\big)F\big(|\mathbf{r}'-\mathbf{r}|\big)\\ \approx \int \mathrm{d}\mathbf{r}'\big(\mathbf{r}'-\mathbf{r}\big)\cdot\nabla f(\mathbf{r})(\mathbf{r}'-\mathbf{r})F\big(|\mathbf{r}'-\mathbf{r}|\big)\\ =\nabla f(\mathbf{r})+O(3).\end{aligned} \tag{1}$$

Here, $f(\mathbf{r})$ could be a function that describes the fluid and $F(\mathbf{r})$ has the following property, $\int \mathrm{d}\mathbf{r}F(r)\mathbf{r}\mathbf{r}=\mathbf{1}$. Additional relationships and properties of $F(\mathbf{r})$ are described in the Appendix. This integral is an alternate representation of the gradient of the function $f(\mathbf{r})$ up to O(3) in gradients. The next step is to approximate this integral as a summation over neighboring points noting that to each point, $\mathbf{r}_q$, there is associated a fluid property, f_q. Consider, first, a "smoothed" representation of $f(\mathbf{r})$, given as

$$f(\mathbf{r})=\sum_q f_q S\big(|\mathbf{r}_q-\mathbf{r}|\big) \tag{2}$$

with

$$S\big(\mathbf{r}_q-\mathbf{r}\big)=\frac{W\big(|\mathbf{r}_q-\mathbf{r}|\big)}{\sum_p W\big(|\mathbf{r}_p-\mathbf{r}|\big)}. \tag{3}$$

Here, $W(|\mathbf{r}_q - \mathbf{r}|)$ is a weight function such that number density of particles, d_p, can be written as

$$d_p = \sum_q W\big(|\mathbf{r}_q - \mathbf{r}_p|\big), \tag{4}$$

thus insuring that the representation of $f(\mathbf{r})$ is properly normalized. The fluid density, ρ_p, at point, $\mathbf{r}_p$, is then given by $\rho_p = m d_p$, where, m, is the mass. It can be shown that the gradient of f at a point labeled p can be written

$$\nabla f_p = \nabla f(\mathbf{r}_p) = \frac{1}{d_p} \sum_q \big(f_q - f_p\big)\big(\mathbf{r}_q - \mathbf{r}_p\big) F\big(|\mathbf{r}_q - \mathbf{r}_p|\big), \tag{5}$$

where $\nabla W(r) = -\mathbf{r} F(\mathbf{r})$. On inspection, it is clear that Eq. 5 is consistent with Eq. 1.

Note, in this paper i and j will be reserved to indicate components of vectors, whereas p and q will correspond to actual SPH particles. Also, there is no distinction between raised or lowered indices.

Using this approach, the time evolution of a fluid may be represented as a set of particles, located at $\mathbf{r}_p$, carrying local fluid properties, that undergo motion in response to effective "interparticle" forces that are defined by a descretized version of an integral representation of the Navier–Stokes equations. To achieve this, consider the Lagrangian formulation of the continuity equation and the general Navier–Stokes equations (Landau and Lifshitz 1987):

$$\frac{\partial \rho}{\partial t} = -\rho \nabla \cdot \mathbf{v}, \tag{6}$$

and

$$\rho \frac{\partial v_i}{\partial t} = -\frac{\partial P}{\partial x_i} + \frac{\partial}{\partial x_k}\left\{\mu\left(\frac{\partial v_i}{\partial x_k} + \frac{\partial v_k}{\partial x_i} - \frac{2}{3}\delta_{ik}\nabla \cdot \mathbf{v}\right)\right\} + \frac{\partial}{\partial x_i}\left(\zeta \nabla \cdot \mathbf{v}\right). \tag{7}$$

Here, ρ, is the fluid density, P is pressure, v is velocity, μ and ζ are the shear and bulk viscosities, respectively. In these equations, the bulk and shear viscosities cannot be taken outside the gradient operator because they can be spatially dependent. In the limit that the viscosity is a constant (Eq. 7) reduces to the usual Navier–Stokes equations. Note, the Lagrangian formulation is preferred because this approach can give us more flexibility in handling moving boundaries as shown in a previous work for the case of a DPD-based model.

Given the result shown in Eq. 5, it is easy to see that a discrete representation of the continuity equation is Monaghan (2005):

$$\left(\frac{\partial \rho}{\partial t}\right)_p = m \sum_q F\big(|\mathbf{r}_p - \mathbf{r}_q|\big)\big(\mathbf{r}_p - \mathbf{r}_q\big) \cdot \big(\mathbf{v}_p - \mathbf{v}_q\big). \tag{8}$$

To construct an integral representation of the general Navier–Stokes equation, a good starting point (Zhu et al. 2010)[1] is to consider the following integral equation:[2]

$$A_i = 5 \int \mathrm{d}\mathbf{r}' \big[\mu(\mathbf{r}') + \mu(\mathbf{r})\big]\big[v^j(\mathbf{r}') - v^j(\mathbf{r})\big] \times \left[\frac{(\mathbf{r}' - \mathbf{r})^i (\mathbf{r}' - \mathbf{r})^j}{(\mathbf{r}' - \mathbf{r})^2}\right] F(|\mathbf{r}' - \mathbf{r}|). \tag{9}$$

Expanding $\mu(\mathbf{r}')$ and $v^j(\mathbf{r}')$ about $\mathbf{r}$ and taking advantage of the properties of $F(r)$ one obtains

$$A_i = \nabla \cdot \big(\mu \partial_i \mathbf{v}\big) + \nabla \cdot \big(\mu \nabla v^i\big) + \partial_i\big(\mu \nabla \cdot \mathbf{v}\big). \tag{10}$$

Incorporating this approximation into Eq. 7 the following result is obtained

$$\rho \frac{\partial v_i}{\partial t} = -\frac{\partial P}{\partial x_i} + A^i + \frac{\partial}{\partial x_i}\left(\left(\zeta - \frac{5}{3}\mu\right)\nabla \cdot \mathbf{v}\right) = -\frac{\partial P}{\partial x_i} + A_i + B_i \tag{11}$$

with $B_i = \frac{\partial}{\partial x_i}\left((\zeta - \frac{5}{3}\mu)\nabla \cdot \mathbf{v}\right)$. Hence to $O(3)$ in gradients, the Taylor expansion of Eq. 9, alone, i.e., $B_i = 0$, recovers the velocity gradient portion of the Navier–Stokes equations with the assumption that $\zeta = \frac{5}{3}\mu$. The SPH representation of A_i is given by

$$A_p^i = 5 \sum_q \frac{F\big(|\mathbf{r}_p - \mathbf{r}_q|\big)}{\rho_q} \times \left[\frac{\big(\mu_p + \mu_q\big)\big(\mathbf{r}_p - \mathbf{r}_q\big)^i \big(\mathbf{r}_p - \mathbf{r}_q\big) \cdot \big(\mathbf{v}_p - \mathbf{v}_q\big)}{\big(\mathbf{r}_p - \mathbf{r}_q\big)^2}\right]. \tag{12}$$

[1] This earlier paper provides an alternate SPH-based construction of the general Navier–Stokes equations by utilizing the representation of gradients, as found in Eq. 1. As a result, obtaining second order derivatives requires repeated application of Eq. 1. The formulation of the general Navier–Stokes equations in the current paper avoids the direct construction of many of the second-order derivatives through the use of Eq. 9.

[2] Note, a similar integral form is used for the heat equation with a spatially dependent thermal conductivity (Monaghan 2005) and for the Navier–Stokes equations with constant viscosity (Español and Revenga 2003).

To incorporate the third term on the right of Eq. 11 so that the ratio of shear to bulk viscosity is not fixed to $\frac{5}{3}$, one may use the derivative of a product property and the following approximations. Taking $a = \zeta - \frac{5}{3}\mu$ then

$$B^i = \frac{\partial}{\partial x_i}(a\nabla\cdot\mathbf{v}) = (\partial_i a)\nabla\cdot\mathbf{v} + a\partial_i\nabla\cdot\mathbf{v}. \tag{13}$$

Using standard SPH-based representations of derivatives and gradients (Monaghan 2005) in Eq. 11, one obtains:

$$\begin{aligned}\left(B_i^a\right)_p &= (\partial_i a)_p \\ &= \frac{m}{\rho_p}\sum_q F\left(|\mathbf{r}_p-\mathbf{r}_q|\right)\left(\mathbf{r}_p-\mathbf{r}_q\right)_i\left(a_p-a_q\right),\end{aligned} \tag{14}$$

$$\begin{aligned}\left(B_i^b\right)_p &= (\nabla\cdot\mathbf{v})_p \\ &= \frac{m}{\rho_p}\sum_q F\left(|\mathbf{r}_p-\mathbf{r}_q|\right)\left(\mathbf{r}_p-\mathbf{r}_q\right)\cdot\left(\mathbf{v}_p-\mathbf{v}_q\right),\end{aligned} \tag{15}$$

and from Español and Revenga (2003), we deduce

$$\begin{aligned}\left(B_i^c\right)_p = \left(a\partial_i\nabla\cdot\mathbf{v}\right)_p = ma_p\sum_q\frac{F\left(|\mathbf{r}_p-\mathbf{r}_q|\right)}{\rho_q} \\ \times\left[5\left[\frac{\left(\mathbf{r}_p-\mathbf{r}_q\right)^i\left(\mathbf{r}_p-\mathbf{r}_q\right)\cdot\left(\mathbf{v}_p-\mathbf{v}_q\right)}{\left(\mathbf{r}_p-\mathbf{r}_q\right)^2}\right]-\left(\mathbf{v}_p-\mathbf{v}_q\right)^i\right],\end{aligned} \tag{16}$$

so that

$$B_p^i = \left(B_i^a\right)_p * \left(B_i^b\right)_p + \left(B_i^c\right)_p. \tag{17}$$

An alternative representation would be to determine $a\nabla\cdot\mathbf{v}$ for each SPH particle and then apply the gradient representation in Eq. 5. However, the Eq. 17 version will be used for this work. Note that the term, $\nabla\cdot\mathbf{v}$, can be directly obtained from evaluation of the continuity equation so that no additional calculation is needed.

To account for the pressure gradient term, we follow the previous work of Monaghan (2005):

$$(\nabla P)_p = -m\rho_p\sum_q\left(\frac{P_p}{\rho_p^2}+\frac{P_q}{\rho_q^2}\right)F\left(|\mathbf{r}_p-\mathbf{r}_q|\right)\left(\mathbf{r}_p-\mathbf{r}_q\right). \tag{18}$$

A pressure term, commonly used to model incompressible fluids, is given as $P = c^2(\rho-\rho_{\text{eq}})$ where c is related to the speed of sound and ρ_{eq} is an equilibrium density.

When determining the local value of the viscosity it will be first necessary to evaluate the local shear rate tensor. A representation of the discretized shear rate is given by:

$$\left(\dot\gamma_{ij}\right)_p = \sum_q\frac{F\left(|\mathbf{r}_p-\mathbf{r}_q|\right)}{\rho_q/m}\left(\mathbf{r}_p-\mathbf{r}_q\right)_i\left(\mathbf{v}_p-\mathbf{v}_q\right)_j. \tag{19}$$

The local magnitude of the shear rate is then

$$\dot\gamma_p = \sqrt{\frac{\sum_{ij}\left(\dot\gamma_{ij}\right)_p^2}{2}}. \tag{20}$$

Note that in the limit of constant viscosity, the momentum equations are the same as those derived by Español and Revenga (2003), so this approach is a slight generalization of theirs. In another work (Monaghan 2005), the B_i term is missing, which, again, is the same as taking $\zeta = \frac{5}{3}\mu$ or $a = 0$. In this work, we will take the bulk viscosity as zero, that is, we set $a = -\frac{5}{3}\mu$. Including the bulk viscosity, as in previous models (Monaghan 2005), by effectively taking the parameter $a = 0$, can introduce oscillations in the flow field which is not studied this paper.

Model for rigid body inclusions

The model for colloidal particles largely follows that used for DPD-based simulations in Hoogerbrugge and Koelman (1992) and Martys (2005). As in the case of the DPD-based models, a colloid is defined as an assembly of constrained SPH particles so that they form a rigid body. The rigid body motion is then determined by summing the forces due the neighboring SPH particles and other auxillary forces (e.g., lubrication, colloidal and body forces). As described previously in Boek et al. (1997) and Martys (2005), when modeling a dense suspension of hard spheres, DPD, or in this case SPH, particle interactions are not sufficiently strong enough to prevent overlaps of the colloidal spheres. To model realistic flows between neighboring spheres in very close proximity would require a very fine resolution, or a number density of particles that is too high to make simulations tractable over reasonable times. To avoid this problem, lubrication forces (Kim and Karrila 1991; Martys 2005) are explicitly included in the simulation to account for hydrodynamic interactions between neighboring spheres. There are several forms or "modes" of lubrication force interactions between hard spheres. The most well known and important is called the squeeze mode, that accounts for forces that develop as two spheres directly approach each other.

This force is proportional to the velocity difference between the spheres and is inversely proportional to the nearest surface-to-surface distance. For the case of monosize spheres, the lubrication force, $\mathbf{F}_{\text{lub}}$, is equal to $\frac{3}{2}\pi\mu a_r^2(\mathbf{V_A}-\mathbf{V_B})/s_{AB}$, where a_r is the sphere radius, $\mathbf{V_A}$ and $\mathbf{V_B}$ are the velocities of spheres "A" and "B", and s_{AB} is the nearest surface to surface distance between spheres labeled A and B. There are additional contributions to the squeeze mode as well as other modes like the twist mode, which, as it sounds, describes the effect of one sphere rotating relative to a neighboring sphere. These additional contributions all scale logarithmically and are largely dominated by the squeeze mode.

For the case of hard spheres, all the modes of the lubrication force, up to the first order, including terms that scale as $1/s_{AB}$, $\ln s_{AB}$ and $s_{AB}\ln s_{AB}$, will be used in simulations. When the colloidal particle is not spherical, the lubrication force must be modified to account for local curvature. In this case the lubrication force is limited to the squeeze mode for this paper.

An additional modification of the lubrication force is made by adjusting the viscosity of the lubrication force term to account for the local shear rate between rigid bodies near the sphere surface. This modification is admittedly heuristic, however, as a first approximation of shear-thinning effects of two rigid bodies in near contact, may be considered reasonable. Further study of this effect is needed.

Although lubrication forces will prevent overlaps of spheres, it is well known that in the course of a simulation such rigid bodies are not restricted from extremely close approaches. When the spheres are nearly in contact, very refined time steps are needed such that the simulation becomes too time consuming. To avoid this problem, yet still account for the lubrication force effects, a short range repulsive force, $F_{AB}\sim\frac{C}{s_{AB}^8}$, directed radially between colloids A and B, was included in the simulation. The functional form of repulsion is akin to a DLVO approximation of a Lennard–Jones hard sphere repulsion force (Israelachvili 1992).

All simulations will be carried out in the limit of low Reynolds number. $\text{Re}=\rho Lv/\mu=\rho a_r^2\dot{\gamma}/\mu << 1$ where, a, is the sphere radius. As there are no thermal fluctuations present in this simulation, the results will correspond to the infinite Peclet number limit.

Numerical integration approach

A modified velocity Verlet time integration algorithm is used for both the "fluid" particles and the rigid body inclusions (Groot and Warren 1997; Martys 2005; Martys and Mountain 1999). The basic algorithm is given in the following equations for an incremental time step δt:

$$x(\delta t)=x(0)+v(0)\delta t+\frac{\delta t^2}{2}a(0), \tag{21}$$

$$v(\delta t)=v(0)+\frac{\delta t}{2}\big[a(0)+a(\delta t)\big], \tag{22}$$

where $a(0)=f(x(0),\tilde{v}(0))/m$ is the acceleration of the SPH particle due to an effective force f described in the next section and $\tilde{v}$ is taken to be (Groot and Warren 1997)

$$\tilde{v}(\delta t)=v(0)+\frac{\delta t}{2}a(0). \tag{23}$$

The translation of the rigid body inclusion was also updated using a similar modified velocity-Verlet approach while a quaternion based algorithm accounted for the rotation of the object. Details of this algorithm are beyond the scope of this paper and are given in Martys and Mountain (1999). It should be mentioned that this approach has been used in previous studies of suspension flow based on the DPD method. The SPH-based computational model described in this paper is similar in structure to that of DPD so that it was relatively easy to adapt the SPH model into the DPD-based code.

Stress tensor

To evaluate the rheological properties of the composite fluid (i.e., fluid matrix and rigid bodies combined), it is convenient to construct a stress tensor based on Kirkwood's approach and similar to that used in molecular dynamics and DPD (Hoogerbrugge and Koelman 1992; Martys 2005; Allen and Tildesley 1987). We first rewrite:

$$m\left(\frac{\partial v_i}{\partial t}\right)_p=\frac{m}{\rho_p}\left[-\left(\frac{\partial P}{\partial x_i}\right)_p+(A_i)_p+(B_i)_p\right], \tag{24}$$

as

$$m\left(\frac{\partial v_i}{\partial t}\right)_p=\sum_{q\neq p}f_{pq}^i, \tag{25}$$

where m is a mass that will be taken to equal 1 in the simulation. We can think of each neighboring SPH particle, labeled q, contributing a force $\mathbf{f}_{pq}$ on SPH particle, p, as all terms on the right side of Eq. 19 result

from a summation over the neighboring particles. The stress tensor for this model suspension has several contributions. There are contributions from the propagation of momentum and inter-particle forces of the SPH particles that are given by

$$\sigma_{ij} = \frac{1}{V_t m}\sum_q \tilde{p}_i^q \tilde{p}_j^q + \frac{1}{2V_t}\sum_{p,q} f_{pq}^i (r_p - r_q)_j, \tag{26}$$

where $\tilde{p}^q$ is the momentum of particle q relative to the macroscopic velocity field and V_t is the total volume of the system. There are corrections to the stress tensor due to the constraint forces on the SPH particles that make up the colloid. The constraint forces are determined by accounting for the rigid body motion in the individual particles displacements and change in velocity at each time step of the velocity-Verlet algorithm. Determination of the correction for constraint forces is described in Martys and Mountain (1999).

In addition, there are contributions to the stress tensor from the colloidal particle interactions. The stress contribution from a central force between spherical bodies is given by

$$\sigma_{ij}^c = \frac{1}{2V}\sum_{A,B} F_{AB}^i (r_A - r_B)_j, \tag{27}$$

where A and B refer to two different colloids and F_{AB} is the force between colloids particles A and B described above. Stress calculations from lubrication forces are also included. The forms of these equations are described in Kim and Karrila (1991). The viscosity of the entire system is then obtained from evaluation of the total stress tensor $\mu = \sigma_{xy}/\dot{\gamma}$.

For the simulations in the study, the number density of SPH particles ranged from 3 to approximately 4.6 (where length is defined in units of h, see Appendix). For a simple Couette flow the lower value was adequate to reproduce the correct viscosity as a function of shear rate. To improve resolution for the spheres simulation, the higher value of density was used.

For the case of simulating Couette flow, a Lees–Edwards Allen and Tildesley (1987) boundary condition was utilized. This boundary condition is equivalent to application of a constant rate of strain at the boundaries. Other boundary conditions will be described as utilized.

Regularized Bingham fluid

A simple model non-Newtonian fluid of Papanastasiou (1987) was used for preliminary testing of this model. For this model the shear rate dependent viscosity is given by

$$\mu_p = \mu_{\text{pl}} + \frac{\mu_0}{M}\frac{\left[1 - \exp\left(-M\dot{\gamma}_p\right)\right]}{\dot{\gamma}_p}, \tag{28}$$

where μ_{pl} is the viscosity in the limit of infinite shear rate, usually called plastic viscosity, $\mu_0 + \mu_{\text{pl}}$ is the viscosity in the limit of zero shear rate. The factor M, can be thought of as a time scale where the suspension recovers its low shear rate behavior. Although approximating a Bingham fluid, this model actually has a zero yield stress. This model can be thought of as a regularization of the Bingham model, which avoids the singularity in viscosity in the limit of zero shear rate. Unlike viscoelastic fluids, there is no inherent memory effect in this fluid as the viscosity is known immediately from the local shear rate. Such effects have been considered elsewhere for model SPH fluids and could be incorporated into this approach.

A dimensionless number called the Bingham number is given as $Bn = \frac{\mu_0 L}{M\mu_{\text{pl}} V}$ where L is the simulation cell width and V is a characteristic velocity. For the case of Couette flow $\frac{V}{L} = \dot{\gamma}$.

Results

Couette flow

As a first test of this simulation approach, the case of Couette flow is studied for the model of Papanastasiou with a $Bn = 0.1$. Figure 1 shows early and latter stage flow fields for this model fluid. Note, due to the application of the Lees–Edwards boundary condition, there is a higher shear rate near the region of the initial application of the shear, thus causing the fluid to temporarily have a lower viscosity there. On the other hand, because the fluid is more viscous at low shear rates, there is much less flow in the middle portion of the simulation cell making the flow profile appear flat there. However as time progresses the entire fluid evolves to the same shear rate and a linear velocity profile finally develops. The evaluation of the stress tensor for this latter stage flow produces a viscosity consistent with that given by the constitutive relation. Similar results were obtained for other values of Bn.

Poiseuille flow

A second test was to study Poiseuille flow, where a body force-driven flow between parallel plates is

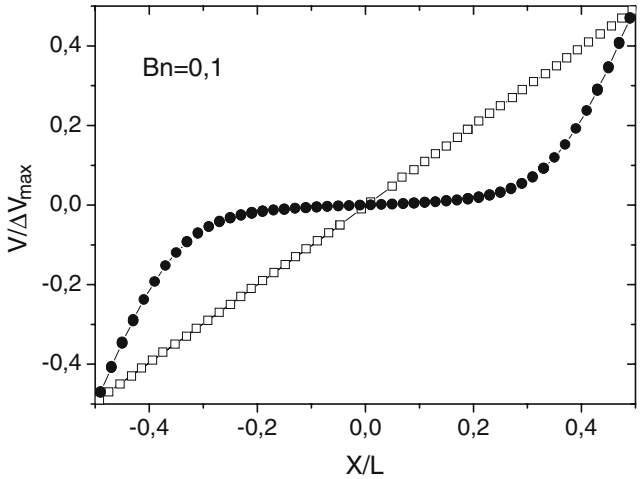

Fig. 1 Velocity profile, normalized to the maximum velocity difference across the simulation cell, $V/\Delta V_{max}$, of width, L, for Couette flow at early (*filled circles*) and late stage (*open squares*) flow. X is the distance from the zero velocity plane in the simulation cell. Note for the early stage flow, near the application of shear on the *left* and *right* hand sides of figure, the shear rate is higher so that the viscosity is lower here. In the *middle* region, at early stages, the velocity profile is more so horizontal as the viscosity is higher here. At later stages of flow, the velocity profile becomes linear

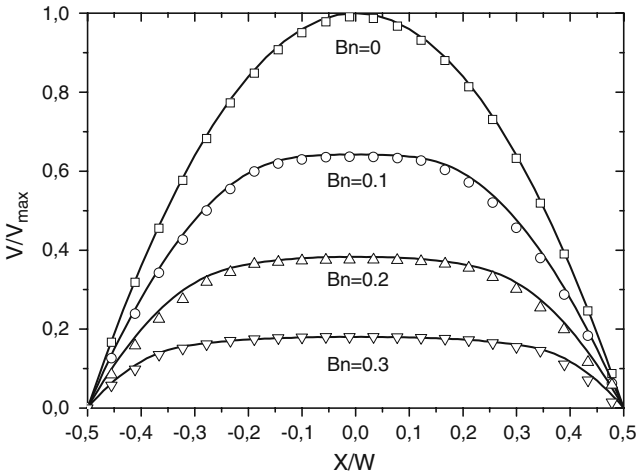

Fig. 2 Equilibrium Poiseuille flow fields for different Bn. The *open symbols* represent results from SPH simulations. The *solid lines* are numerical solutions of the generalized Navier–Stokes equations. W is the width of the cell and X is the distance from the center line of symmetry of the cell. The velocity, V, is normalized to the maximum velocity of the case of $Bn = 0$. The $Bn = 0$ case corresponds to the Newtonian fluid solution which is parabolic. As *Bn*, increases the central portion of the velocity profiles becomes flattened

modeled. This requires the introduction of a no-slip boundary condition at the fluid plate interface. To do this, the following method described in Martys (2005) is utilized. Here, the simulation cell is divided in half and a body force is applied in one direction, in one half of the simulation cell, and in the opposite direction in the other half. Figure 2 shows the velocity profile in a half cell for a set of *Bn*. Also shown is the numerical solution of the general Navier–Stokes equation using the same constitutive equation. Again agreement between simulation and numerical solution is reasonably good. Note that there is a small variation on either side of the velocity profile near the "walls". This example illustrates the sensitivity of the simulation to resolution and is worth indicating. This artifact is a consequence of not using a perfectly symmetric initial configuration of points in the simulation cell. While slightly different velocity profiles are obtained the agreement is still very good with the independent numerical solution, thus demonstrating the robustness of algorithm.

Suspension with an idealized Bingham fluid

Next, some general features of suspension flow for the regularized Bingham model of Papanastasiou (1987) will be discussed. Parameters for the Papanastasiou model were chosen such that the viscosity limit for the low shear rate regime was about 100 times greater than the high shear rate regime. For many cases this model parameter choice would be a good approximation of a Bingham fluid. Figure 3 shows the viscosity of the fluid normalized to the infinite shear-rate value of the viscosity. A set of monosize spheres, making a solid volume fraction of 0.40, are added to the simulation cell. Figure 3 also shows the relative viscosity of this suspension. Again, the suspension viscosity is given relative to the infinite shear rate value of the matrix fluid. While the general trend is that the viscosity of the suspension decreases with shear rate, there are three regimes of interest for this study. Consider comparison of the suspension viscosity with that of the matrix fluid for the same shear rate. If the matrix fluid was Newtonian, the suspension viscosity should be about a factor of ten higher than that of the matrix fluid (Foss and Brady 2000; Martys 2005). Note that at the very low or very high shear rates studied, this limit is being approached in the simulation. The reason is that, at the highest shear rates, the relevant viscosity values sampled through out the simulation cell correspond to the high shear rate limit of the matrix fluid. Other regions in the suspension do not contribute as significantly to the overall stress in the system. A similar argument can be made at the lowest shear rate regime where the viscosity will not vary as much through out the

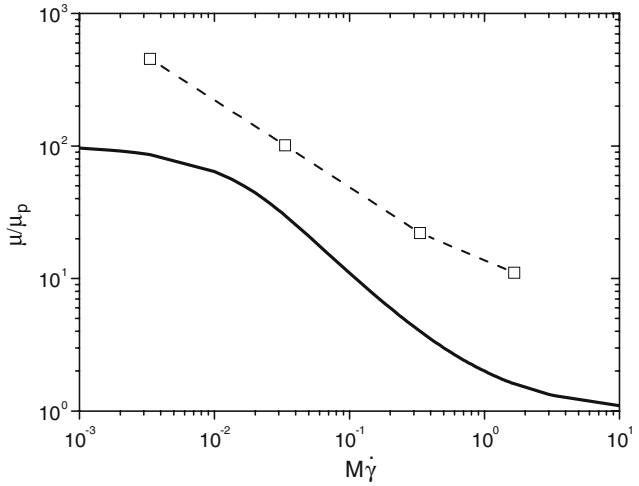

Fig. 3 Comparison of matrix fluid viscosity (*solid line*) and relative viscosity of a suspension composed of monosize spheres with volume fraction 0.40 (*open squares*). Values of viscosity, μ, for both the matrix fluid and suspension are normalized to the plastic viscosity μ_p of the matrix fluid. The matrix fluids properties are based on the regularized Bingham model of Papanastasiou (1987). Parameters for the model were chosen such that viscosity increased by a factor of 100 as the shear rate decreases. The *open squares* represent simulation data for the sphere suspension. At the lowest and highest shear rates, the relative viscosity approaches that of a similar sphere suspension in a Newtonian fluid (approximately a factor of 10 higher than the matrix fluid). At the intermediate shear rates shown, the relative viscosity of the suspension is only about a factor of 2 to 3 higher than the corresponding matrix fluid viscosity

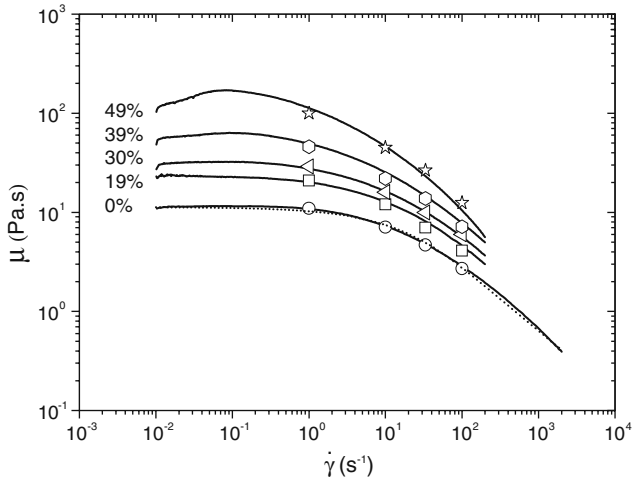

Fig. 4 Comparison of experimental measurements (*solid lines*) of viscosity, μ (Pa-s) as a function of the shear rate $\dot{\gamma}$, (1/s) for a shear-thinning fluid and suspensions composed of silica sphere at the designated volume fractions ϕ with simulation data. The *dashed line* represents a fit to the experimental measurement of the matrix fluid. The *open symbols* represent simulation data. Based on sample preparation, experimental results varied less 10% from that shown in the figure

suspension. An interesting shear rate regime is away from where the viscosity plateaus. Here, the suspension viscosity is only about a factor of two to three higher than the matrix viscosity at each shear rate. In this case, it is found that, as the suspension is sheared, the local shear rate between spheres is much higher than that of the bulk or global shear rate. As a result, the viscosity between the spheres takes on the high shear rate limit so that the overall viscosity is lower than that expected for the relative viscosity.

Comparison with experimental measurements of suspensions with spherical silica particles

Now, comparison is made between simulation and actual experiments on idealized sphere suspensions, Firstly, a shear- thinning fluid was prepared using a solution of 5% by volume Methylhydroxypropylcellulose in water. This fluid has some similarity with the regularized Bingham fluid with a viscosity plateau at low shear rates. However, for the data obtained, there was no indication of a plateau at the highest shear rates tested. Experimental data were obtained with an Anton Paar rheometer[3] either with a cone/plate (50 μm gap) or with a plate/plate (1 mm gap) geometry of 25 mm diameter. Rheological measurements were then made on systems composed of the same matrix fluid but with silica particles added for a set of volume fractions ranging from 0.19 to 0.49. The silica particles are type P0060-Beads with diameter ranging between 100 to 140 μm. Figure 4 shows the viscosity as a function of shear rate of the matrix fluid and the suspension made by adding the silica spheres to the matrix fluid. Tests were performed to check for the influence of sedimentation and migration on the measured viscosity. We expected that effects due to sedimentation would be small due to the relatively high viscosity of the matrix fluid. As a check, measurements were made at a fixed shear rate for two minutes and did not show a significant change in viscosity Repeating the measurements with the same sample gave similar results. We also found there was no hysteresis of the viscosity as a function of shear rate when increasing and then decreasing the shear rate. This indicated there was no

[3]Certain commercial equipment, instruments, or materials are identified in this paper in order to specify the experimental procedure adequately. Such identification is not intended to imply recommendation or endorsement by the National Institute of Standards and Technology, nor is it intended to imply that the materials or equipment identified are necessarily the best available for the purpose.

significant sedimentation or migration of the particles over the time scales of the measurement.

The viscosity versus shear rate for the experimental matrix fluid was then fit to a function that was used to define a constitutive law for the fluid. This function was used in the simulation code to define the local viscosity for a given shear rate. Figure 4 shows that the correct viscosity is self consistently recovered by simulation. Next spheres were added to the simulation cell at volume fractions close to that of the experiment. As can be seen in Fig. 4, the simulation results follow the experimental trends closely. Note, at the lowest shear rates, the viscosity of the sphere suspensions, for different volume fraction, are consistent with that of that of a suspension with a Newtonian fluid (Foss and Brady 2000) as the viscosity being sampled is approaching its plateau value. On the other hand, as the shear rates increases, the viscosity of the higher volume fraction suspensions had a tendency to decrease at lower values of shear rate than the lower volume fraction systems. This is a result, for the higher volume fraction suspension, of the typical spacing between spheres being smaller—hence, larger relative shear rates are present between spheres that result in lower localized viscosities.

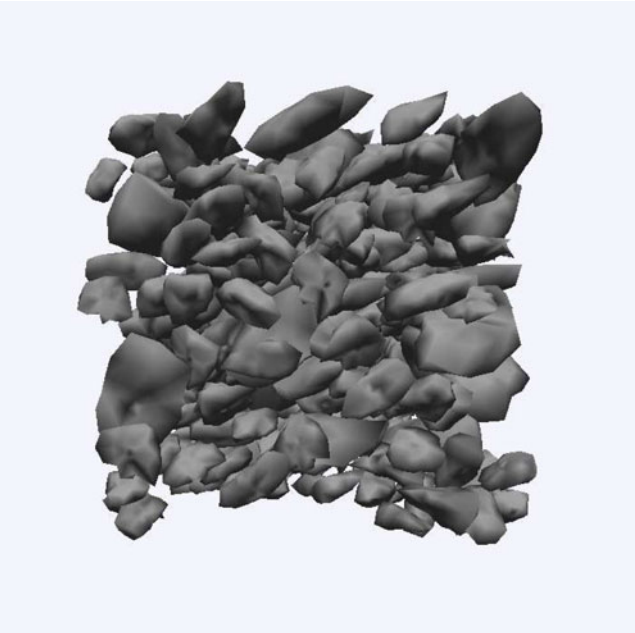

Fig. 5 Visualization of aggregates used in simulation of a suspension composed of sand embedded in a calcium carbonate paste. The volume fraction $\phi = 0.50$. The sand shapes are based on X-ray microtomography images of a related sand (Garboczi et al. 2001)

Comparison with experimental measurements of a model mortar suspension

A second fluid system was considered that is representative of many suspensions (i.e., cement based materials). Here the matrix fluid was calcium carbonate/water slurry with a sand (F-95 (US silica)) added to make a mortar like suspension. Of course the calcium carbonate slurry is also a suspension but the constituent particle sizes are much smaller (less than 10 μm) than that of sand so that it can be thought of as a continuum fluid. The mean sand size was about 0.2 mm in diameter and ranged about a factor of 5 about the mean. A Bohlin CVO coaxial cylinder rheometer with a gap of about 2.5 mm was used to measure the suspension viscosity. In contrast to the previous data, the matrix fluid did not show a plateau in viscosity at lowest shear rates tested, but, did begin to indicate a viscosity plateau at the higher shear rates. As in the previous case the simulation reproduced the correct constitutive relation for the matrix fluid. A model for the sand particles was used in the simulation that was based on reconstructed tomographic images (Garboczi et al. 2001) of a similar sand (Fig. 5). The tomographic images were analyzed so that the local surface properties (surface normals, principle curvature) of the particles could be incorporated into the simulation in order to better estimate lubrication forces. For the two volume fractions studied (0.40 and 0.50) there was good agreement (Fig. 6) between simulation and experiment, especially given that

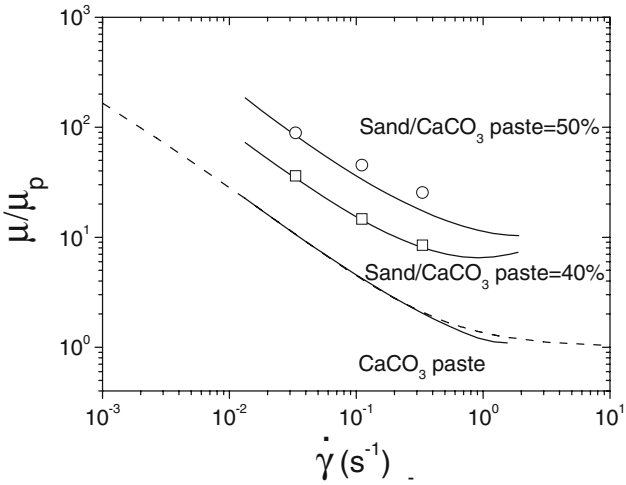

Fig. 6 Comparison of simulation (*open symbols*) results to experimental measurements (*solid lines*) of relative viscosity, vs shear rate $\dot{\gamma}$, (1/s) for a suspension composed of sand embedded in a calcium carbonate paste. The matrix fluid (*bottom solid line*) and an approximate fit (*dashed line*) to the data are also shown. Data for volume fractions $\phi = 0.40$ and 0.50 are shown. Based on sample preparation, experimental results could vary about 10% from that shown in the figure

the model inclusions were not necessarily identical to the sand particles. Note the higher values obtained for the simulation for the 0.50 volume fraction could in part be attributable to a sensitivity of particle shape variation in the simulation. Clearly more study is needed here but the results are encouraging.

Conclusion

In conclusion, a set of numerical equations for modeling suspensions with a non-Newtonian fluid matrix has been presented. In a series of tests of this model, very good agreement was found between simulation and independent numerical solutions, and, with a set of experiments performed on two different suspensions. This work demonstrates that one may measure the rheological properties of a fluid and then use this measurement as input into a simulation code to determine the properties of a suspension having the same matrix fluid. Extending this model to other fluid types (e.g., viscoelastic, temperature dependent viscosity...) is straight forward. Further research is needed to better understand how to properly modify lubrication forces to account for the presence of a non-Newtonian fluid matrix. In addition, correct modeling of thermal fluctuation effects to account for low Peclet number flow would also be desirable as this is not currently understood for the case of a non-Newtonian fluid.

Acknowledgements We would like to gratefully acknowledge support from the Virtual Cement and Concrete testing Laboratory Consortium (VCCTL). The flow simulations were performed under award SMD-05-A-0129, "Modeling the Rheological Properties of Suspensions: Applications to Cement Based Materials" for NASA's National Leadership Computing System Initiative on the "Columbia" supercomputer at the NASA Ames Research Center. This research also used resources of the Argonne Leadership Computing Facility at Argonne National Laboratory, which is supported by the Office of Science of the US Department of Energy under contract DE-AC02-06CH11357.

Appendix

Proper construction of the weight function $W(r)$ is important for the physically correct transmission of matter or forces between neighboring SPH particles. Here some key properties of $W(r)$ and its derivative are given for convenience. The weight function and alternate formulations are discussed more fully in Español and Revenga (2003), Monaghan (2005).

$$\int d\mathbf{r} W(r) = 1. \tag{29}$$

$$\nabla W(r) = -\mathbf{r} F(r) \tag{30}$$

In this work, the SPH Lucy function is utilized for a weight function.

$$W(r) = \frac{105}{16\pi h^3}\left(1 + 3\frac{r}{h}\right)\left(1 - \frac{r}{h}\right)^3 \tag{31}$$

and

$$F(r) = \left(\frac{315}{4\pi h^5}\right)\left(1 - \frac{r}{h}\right)^2. \tag{32}$$

For for the remainder of this paper, we set $h = 1$. Some of the more important properties of $F(r)$ are given below.

$$\int d\mathbf{r} F(r)\mathbf{rr} = \mathbf{1}. \tag{33}$$

$$\int d\mathbf{r} F(r)\frac{xxxx}{r^2} = \frac{3}{5}. \tag{34}$$

$$\int d\mathbf{r} F(r)\frac{xxyy}{r^2} = \frac{1}{5}. \tag{35}$$

References

Allen MP, Tildesley DJ (1987) Computer simulation of liquids. Claredon, Oxford

Barnes HA (1989) Shear-thickening ("dilatancy") in suspensions of non-aggregating solid particles dispersed in Newtonian liquids. J Rheol 33(2):329–366

Bender J, Wagner NJ (1996) Reversible shear thickening in monodisperse and bidisperse colloidal dispersions. J Rheol 40(5):899–916

Boek E, Coveney PV, Lekkerkerker HN, van der Schoot P (1997) Simulating the rheology of dense colloidal suspensions using dissipative particle dynamics simulations. Phys Rev E 55:3124–3133

Español P, Revenga M (2003) Smoothed dissipative particle dynamics. Phys Rev E 67:026705

Fielding SM, Olmsted PD (2004) Spatiotemporal oscillations and rheochaos in a simple model of shear banding. Phys Rev Lett 92:084502

Flatt RJ, Martys N, Bergstrom L (2004) The rheology of cementitious materials. MRS Bull 29(5):314–318

Foss DR, Brady JF (2000) Structure, diffusion, and rheology of Brownian suspensions by Stokesian dynamics simulations. J Fluid Mech 407:167–200

Garboczi EJ, Martys NS, Saleh HH, Livingston RH (2001) Acquiring, analyzing, and using complete three dimensional aggregate shape information. In: Aggregates, concretes, bases and fines, ninth annual symposium proceedings (CD-ROM). International center for aggregate research, April 22–25, 2001. Austin Texas, pp 13

Gingold RA, Monaghan JJ (1977) Smoothed particle hydrodynamics: theory and application to non-spherical stars. Mon Not R Astron Soc 181:375–389

Groot RD, Warren PB (1997) Dissipative particle dynamics: bridging the gap between atomistic and mesoscopic simulation. J Chem Phys 107:4423–4435

Hoogerbrugge PJ, Koelman JMVA (1992) Simulating microscopic hydrodynamic phenomena with dissipative particle dynamics. Europhys Lett 19:155:96–160

Israelachvili JN (1992) Intermolecular and surface forces. Academic Press

Kim S, Karrila SJ (1991) Microhydrodynamics. Butterwort–Heinemann

Landau LD, Lifshitz EM (1987) Fluid mechanic. Pergamon, Oxford

Larson RG (1999) The structure and rheology of complex fluids. Oxford University Press, New York

Lootens D, Van Damme H, Hébraud P (2003) Giant stress fluctuations at the jamming transition. Phys Rev Lett 90: 178301

Lucy LB (1977) A numerical approach to the testing of the fission hypotheses. Astron J 82:1013–1024

Martys NS (2005) Study of a dissipative particle dynamics based approach for modeling suspensions. J Rheol 49:401–424

Martys NS, Mountain RD (1999) Velocity Verlet algorithm for dissipative-particle-dynamics-based models of suspension. Phys Rev E 59:3733–3736

Moller PCF, Mewis J, Bonn D (2006) Yield Stress and thixotropy: on the difficulty of measuring yield stresses in practice. Soft Matter 2006 2:274–283

Monaghan JJ (2005) Smoothed particle hydrodynamics. Rep Prog Phys 68:1703–1759

Papanastasiou TC (1987) Flows of materials with yield. J Rheol 31:385–404

Zhu H, Martys NS, Ferraris C, DeKee D (2010) A numerical study of the flow of Bingham-like fluids in two-dimensional vane and cylinder rheometers using a smoothed particle hydrodynamics (SPH) based approach. J Non-Newton Fluid Mech 165:362–375